xGEO Space Domain Awareness:
Parametrization and Characterization of Cislunar Space

Pablo Machuca, Aaron J. Rosengren
Department of Mechanical and Aerospace Engineering, University of California San Diego, USA
Shane D. Ross
Department of Aerospace and Ocean Engineering, Virginia Tech, USA

ABSTRACT

Maintaining a catalog of resident space objects beyond GEO (xGEO) represents a new challenge for Space Domain Awareness (SDA). With the Lunar Gateway and increased international efforts to explore and exploit the Moon and cislunar space, a plethora of dynamically complex xGEO orbits are expected to be populated in the coming years. This study addressed topics of fundamental significance for the pressing problem of xGEO SDA: i.e., (1) characterization of the dynamical environment and common scenarios of interest; (2) effective and intuitive parameterizations to describe the orbital motion of xGEO objects in this non-traditional orbital environment; and (3) quantification of uncertainties involved in the orbit determination (OD) process. Specifically, we reproduce, in a high-fidelity ephemeris model, common mission scenarios of interest: e.g., (a) transfers between quasi-periodic halo orbits (including that baselined for the Lunar Gateway), and (b) a transfer from a near-rectilinear halo orbit to a distant retrograde orbit. We then propose a parameterization approach to describe such trajectories based on piecewise orbital elements (geocentric or selenocentric, as the physical picture dictates). We show that, despite the non-Keplerian nature of these restricted three-body orbits, the classical elements are still well defined and provide a time-continuous, intuitive and familiar representation of characteristic xGEO trajectories. Additionally, we model and propagate uncertainties involved in the OD process to better understand the inherent sensitives that plague xGEO and their implications for SDA viewing geometries, required revisit rates, and surveillance volumes. Normality of OD uncertainties is maintained for approximately 40 days, clouds of uncertainty remain fully observable and within the nominal field of view of a ground telescope for approximately 80 days, and close encounters with the Earth and Moon are shown to most significantly affect the size and geometry of propagated clouds of uncertainty.

1. INTRODUCTION

Cislunar space is expected to be increasingly populated in the coming decades. The dynamical complexity of the environment and wide range of available orbits pose a significant new challenge for Space Domain Awareness (SDA); namely, the catalog maintenance of xGEO (beyond GEO) objects. The intrinsic stability/instability of orbits, increasingly complex trajectory designs, plethora of station-keeping strategies, and limited visibility windows require a better understanding of this non-traditional orbital environment. Accordingly, we aim to provide: (1) a thorough characterization of the cislunar multi-body dynamical environment geared towards typical scenarios of interest; (2) an intuitive, familiar parametrization to describe the motion of xGEO objects; and (3) an uncertainty quantification analysis of the orbit determination (OD) process, with the overall goal of understanding how uncertainties affect viewing geometries and observation campaigns for catalog maintenance.

Specifically, we reproduce and characterize relevant mission profiles in the Circular Restricted Three-body Problem (CR3BP) and in an ephemeris model, including: (a) transfers between quasi-periodic halo orbits (including the 9:2 resonant near-rectilinear halo orbit baselined for the Lunar Gateway), and (b) transfers into distant retrograde orbits (DROs), which have been proposed as parking orbits for interplanetary missions. We then propose a parameterization approach to describe such trajectories based on piecewise orbital elements (geocentric or selenocentric, as the physical picture dictates). We show that, despite the non-Keplerianity of orbits, the classical elements are still well defined and can provide an intuitive and useful representation of typical xGEO scenarios. Finally, we model and propagate uncertainties involved in the OD process to better understand the inherent sensitivities that plague cislunar space, and

we highlight their implications to viewing geometries, required revisit rates, and surveillance volumes for improved catalogue maintenance.

Preliminary results are summarized herein. The baseline methodology for the computation of trajectories and orbital-element representation is initially described for a series of transfers between halo orbits around the second Earth-Moon Lagrange point (L2), and the analysis of OD uncertainty propagation is then commented in detail for a transfer between a 9:2 resonant near-rectilinear halo orbit (NRHO) to a 13.8-day DRO.

2. COMPUTATION OF SCENARIOS OF INTEREST

The multi-body dynamics of cislunar space offer a wide range of orbits that permit more complex trajectory designs and mission profiles. We begin our analysis by reproducing cislunar trajectories that may be of interest to future missions. As a sample scenario, we consider the family of Southern L2 halo orbits and transfers between such orbits. Halo orbits around L2 have been proposed for payloads supporting lunar exploration and communications [1, 2, 3], including the Lunar Gateway [4, 5], and also as parking orbits for the efficient insertion of satellites into low-Earth orbit [6]. A variety of halo orbits may be employed in the future: from those originating in the vicinity of the Lagrange point, up to NRHOs with closer lunar passages.

As an initial scenario of interest, we consider a spacecraft that is initially stationed along a Southern 9:2 resonant orbit around L2, such as that baselined for the Lunar Gateway, which then transfers to a smaller halo orbit in the vicinity of L2 through a total of 12 intermediate halo orbits (Fig. 1, in synodic reference frame). This scenario may be representative of a spacecraft leaving the Lunar Gateway with the intent of departing the Earth-Moon system through lower-energy orbits [4]. It also allows us to consider a range of halo orbits along the Southern L2 family, including the natural motion along such orbits and transfer maneuvers from/to these orbits.

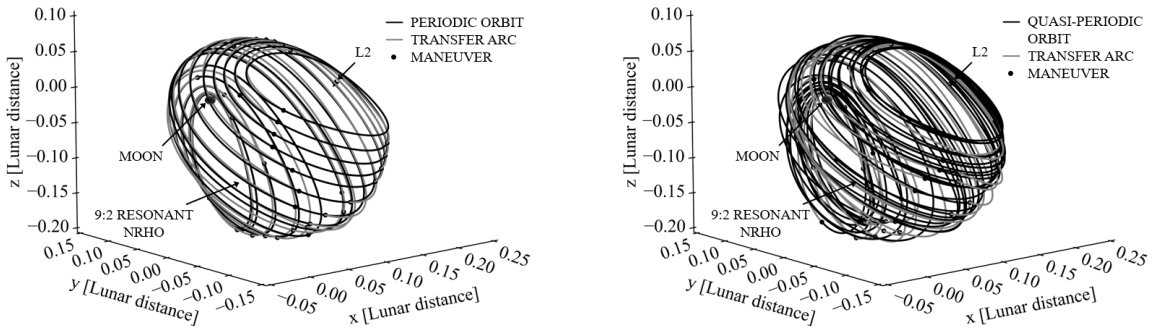

(a) CR3BP model.

(b) Ephemeris model.

Fig. 1: Transfer from an L2 Southern 9:2 resonant NRHO to a smaller halo orbit through a chain of 12 intermediate orbits.

Periodic orbits are initially computed in the CR3BP and then transitioned into quasi-periodic orbits in the ephemeris model (point-mass gravitational effect of the Sun, planets up to Jupiter, and the Moon). This approach allows us to assess the utility of the CR3BP for the identification and characterization of features and general trends, and to identify differences in the orbital-element representation. Furthermore, transfer arcs between halo orbits leverage unstable and stable manifold trajectories associated to the departure and arrival halo orbits: an approach that may become standard in cislunar space. Note, however, that the resulting transfer arcs—departure/arrival trajectories that actually intersect each other in position—are generally close to but may not necessarily remain on the invariant manifolds of the departure/arrival orbits.

It is worth highlighting here that the design of transfer trajectories assumes impulsive maneuvers in both models, but the design process is done separately for the CR3BP and for the ephemeris model. In both models, we leverage invariant manifold dynamics to generate initial guesses for the departure/arrival transfer arcs, but the time of flight along halo orbits and the location of maneuvers, magnitudes, and transfer times may differ between both models. As a result, the whole CR3BP transfer takes a total of 350 days and 612 m/s, and the ephemeris-model transfer takes 556 days and 1041 m/s instead.

Lastly, no claim is made on the optimality of the transfers, and, in fact, it is likely that lower Δv transfers may be found (although of the same order of magnitude). This scenario, nevertheless, allows us to consider a range of maneuver locations (at perilune, apolune, and intermediate points) and magnitudes (between 6 m/s and 35 m/s in the CR3BP, and between 3 m/s and 67 m/s in the ephemeris model).

3. ORBITAL-ELEMENT PARAMETRIZATION

In search of an intuitive parametrization approach to describe the potentially complex motion of xGEO objects, we considered a piecewise representation based on orbital elements: selenocentric if within the Moon's Hill sphere, or geocentric if outside of it. We found that the instantaneously-inertial Earth-Moon synodic reference frame provides the most insightful representation of (quasi-) periodic orbits. It is observed that, in such a frame, the orbital elements describing the shape and size of halo orbits (semi-major axis and eccentricity), and also the elements describing the orbit orientation (inclination, argument of periapsis, and longitude of the ascending node), all display repetitive, nearly-cyclical patterns. Such patterns are perfectly periodic along halo orbits in the CR3BP, and, a similar trend, but not periodic, is observed in the ephemeris model. As an example, Fig. 2 illustrates the behavior of the semi-major axis along the CR3BP and ephemeris-model transfers.

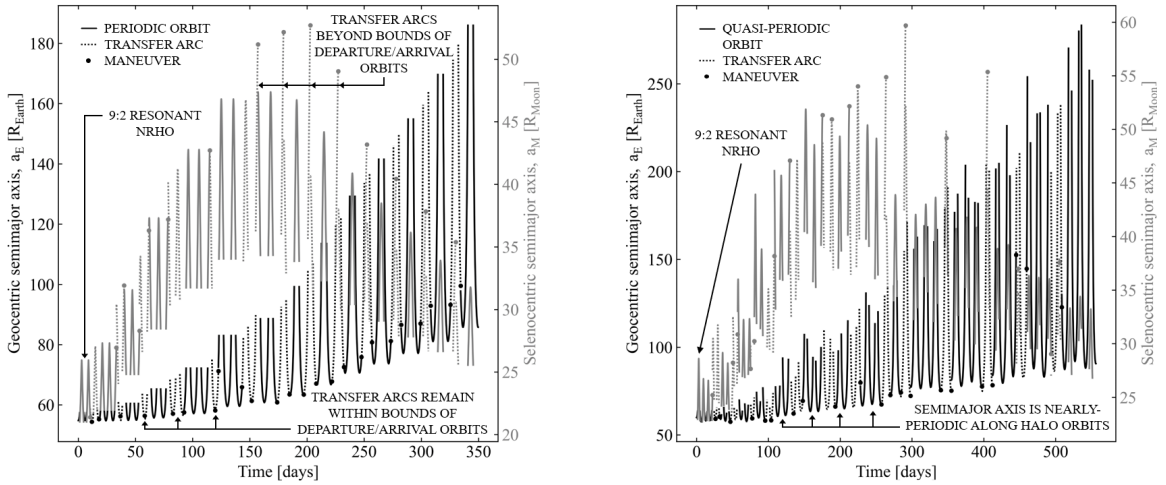

(a) CR3BP model.

(b) Ephemeris model.

Fig. 2: Evolution of geocentric (*left*) and selenocentric (*right*) semi-major axis along chain of halo orbits.

The geocentric semi-major axis is illustrated in black in Fig. 2, and the selenocentric semi-major axis is illustrated in grey. It is observed that a continuous (in time) representation of trajectories can be provided by this piecewise orbital-element parametrization. In particular, long segments along the halo orbits remain outside the Moon's Hill sphere, and the switch to selenocentric elements occurs only at perilune passages.

It is further observed that the oscillation in orbital elements is smaller for orbits closer to the Moon (left-most orbits in Fig. 2), which effectively resemble highly-elliptical circumlunar orbits. For those orbits that are closer to the Lagrange point (right-most orbits), third-body dynamics are more prominent and result in larger orbital-element oscillations. Furthermore, the oscillations in semi-major axis along transfer arcs generally remain within the bounds defined by the departure and arrival orbits: similar to a Hohmann tranfer in the two-body problem, which employs a transfer orbit with semi-major axis equal to the average between the departure and arrival orbits' semi-major axes. This holds true for nearly energy-optimal transfer arcs that remain close to the manifolds. Transfers aiming for shorter-duration arcs, however, may result in semi-major axis oscillations beyond the range imposed by the departure and arrival orbits.

Additionally, maneuvers, which are modeled here as impulsive, are observed to result in instantaneous changes in orbital elements too, and so discontinuities in orbital parameters may be leveraged to identify orbital transfers. As a general trend, it is observed that larger Δv maneuvers may lead to larger changes in orbital elements, but the magnitude of these changes also depends on factors like the direction and location of these maneuvers. For reference, Fig. 3

illustrates the evolution of eccentricity and inclination in the CR3BP and ephemeris models, where similar trends to those exhibited by the semi-major axis are observed.

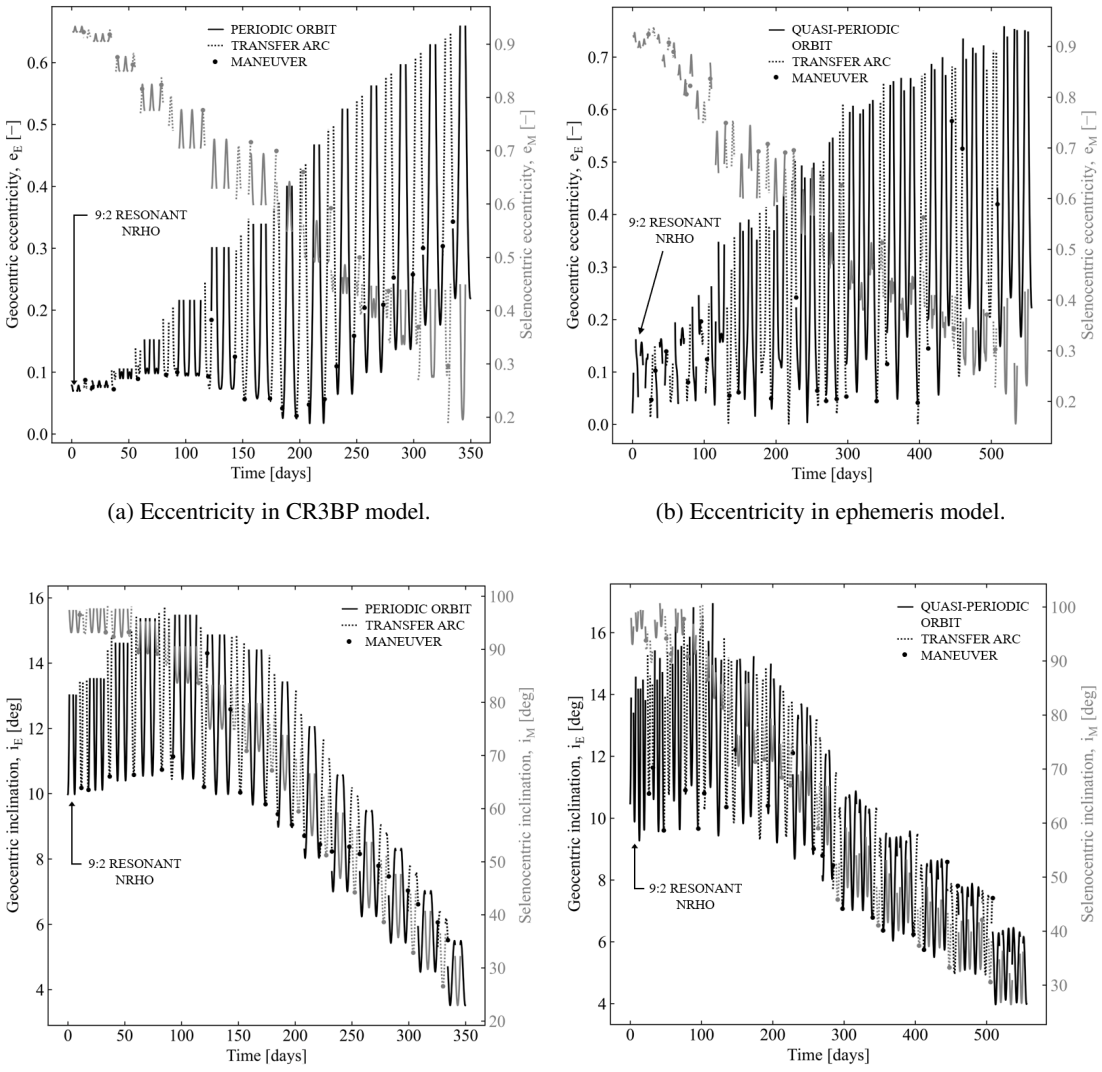

(a) Eccentricity in CR3BP model.

(b) Eccentricity in ephemeris model.

(c) Inclination in CR3BP model.

(d) Inclination in ephemeris model.

Fig. 3: Evolution of geocentric and selenocentric eccentricity and inclination along chain of halo orbits.

A second mission scenario is considered, in which a spacecraft is stationed along a 9:2 resonant NRHO and then performs a transfer into a 13.8-day-period DRO. The geometrical representation of such a scenario is illustrated in Fig. 4 (ephemeris-model trajectory in synodic reference frame), along with the evolution of the piecewise semi-major axis, eccentricity and inclination.

It is observed how the DRO can be fully represented in terms of geocentric orbital elements–since the spacecraft remains outside of the Moon's Hill sphere–and displays oscillatory values of semi-major axis and eccentricity, and a near-zero inclination throughout the periodic orbit. It is again clear how impulsive maneuvers result in instantaneous changes in orbital-element representation, and the orbital elements along the transfer arc may not necessarily remain within the bounds of the departure and arrival orbits.

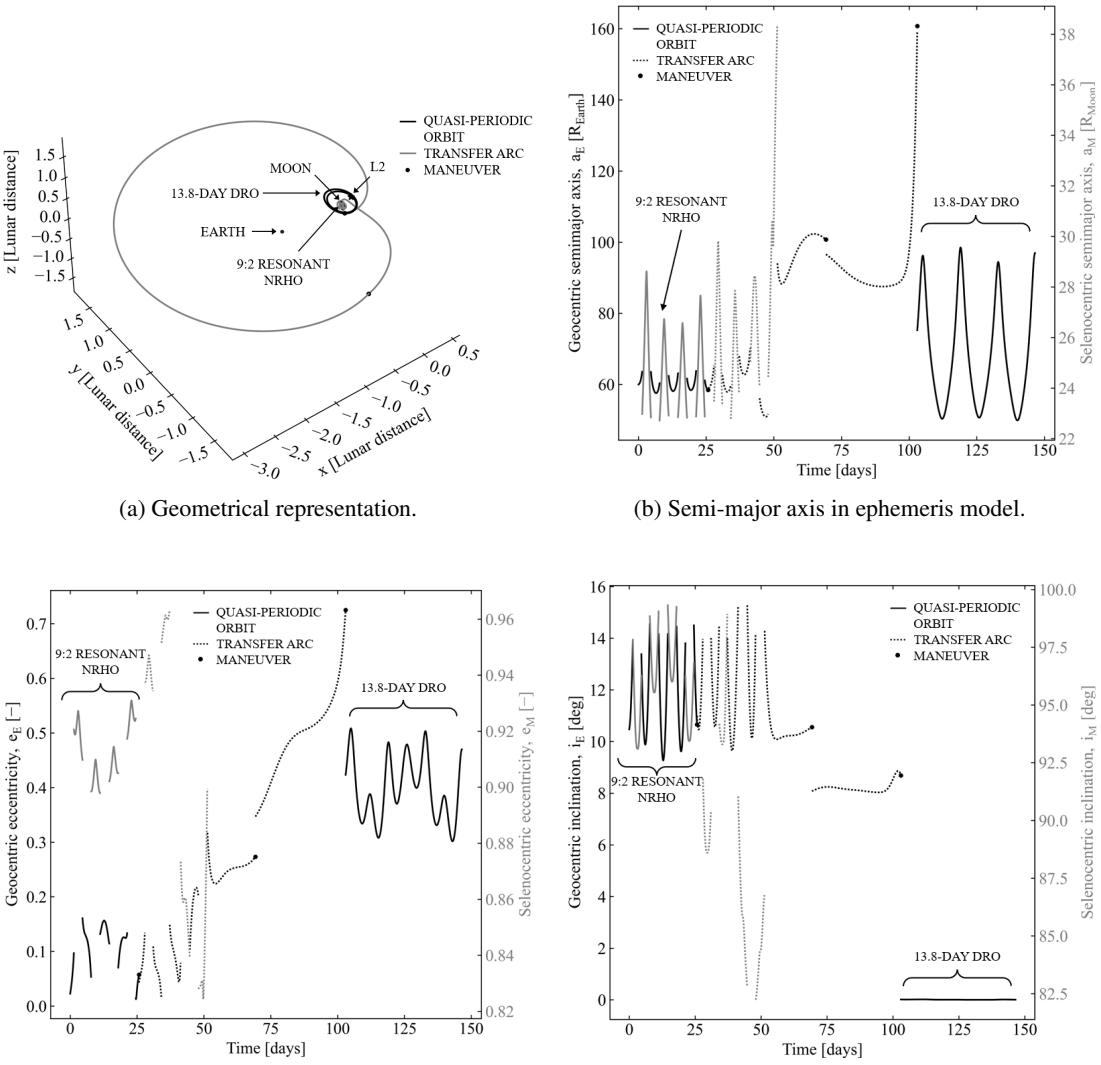

(a) Geometrical representation.

(b) Semi-major axis in ephemeris model.

(c) Eccentricity in ephemeris model.

(d) Inclination in ephemeris model.

Fig. 4: Transfer from an L2 Southern 9:2 resonant NRHO to a 13.8-day-period DRO.

4. ORBIT DETERMINATION AND UNCERTAINTY PROPAGATION

With the goal of understanding how (ground-based) orbit determination uncertainties will propagate with time and how this would affect viewing geometries and required revisit rates, we initially try to gauge the orbit determination accuracies that could be expected along such cislunar scenarios of interest. As an example, we use as reference here the transfer between a 9:2 resonant NRHO to a 13.8-day DRO (Fig. 4). We also assume an initially-cataloged passive spacecraft and that only ground-based optical measurements are available at such far distances from Earth.

A simple extended Kalman filter (EKF) with sufficiently frequent observations (every hour) is employed here to confine the nonlinear effects of the dynamical system. Alternatively, an unscented Kalman filter (UKF), more robust against nonlinearities, with less frequent observations could be employed. Dynamics are assumed to be perfectly known by the EKF and conservative Gaussian noises are introduced in the two measured angles: 4 arcsec (1σ) [7]. Optical observations are assumed to be collected by two ground telescopes located in continental USA and Australia, for proper characterization of the spacecraft's trajectory out of the equatorial plane. Lastly, observations are only possible during nighttime, more than 15 degrees above the horizon, and outside of a 10-degree lunar exclusion zone.

Fig. 5 summarizes the OD results from 10,000 Monte Carlo simulations with randomized measurement noise along the ephemeris trajectory in Fig. 4a.

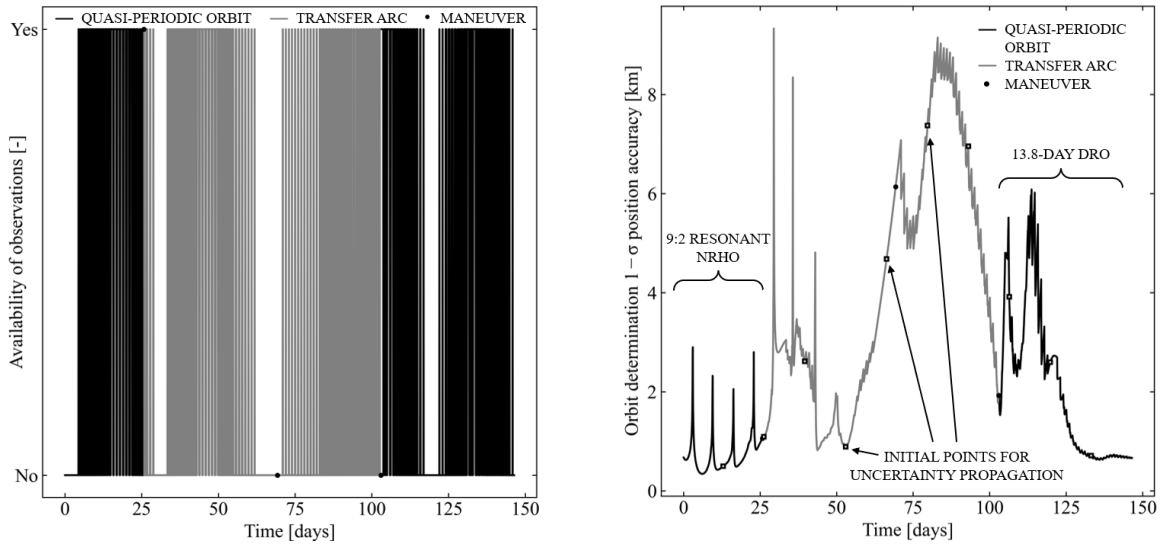

(a) Availability of measurements.

(b) Evolution of OD accuracy.

Fig. 5: Orbit determination process along transfer from L2 Southern 9:2 resonant NRHO to 13.8-day DRO.

Orbit determination accuracies are observed to range from $\sim$0.5 up to $\sim$10 km, but several factors influence these values, for instance: (1) OD inaccuracies increase at close Earth and Moon passages: likely due to unmodeled nonlinearities in the EKF, which could be mitigated by a UKF or more frequent observations in these high-speed regions, (2) OD inaccuracies linearly increase in periods of time without new observations, which also record the largest OD errors, and (3) OD inaccuracies increase at farther distances from Earth (i.e., along the transfer arc).

When looking at the distribution of such inaccuracies (Fig. 6), we observe that OD inaccuracies preserve nearly-normal distributions throughout the trajectory. Fig. 6 illustrates the distribution of x-coordinate positional estimation error (in synodic reference frame) at different points along the trajectory, where a close resemblance to normal distributions can be observed. The aim of the uncertainty propagation analysis is then to answer questions like: if no new observations of the spacecraft are collected, "how long will OD uncertainties remain nearly normal?", or "how long will clouds of uncertainty remain within the nominal field of view?" By "nominal field of view" we refer to the ground telescope's field of view when oriented towards the reference spacecraft position at the time of observation (i.e., ephemeris trajectory in Fig. 4a). A typical 2.0 deg x 2.0 deg field of view is assumed [7], and, if the cloud of OD uncertainty extends beyond this field of view at the time of observation, we consider the ground telescope may need to search for the

spacecraft again (Fig. 7b); if the cloud of uncertainty remains in its totality within the field of view, then the ground telescope would be able to observe the spacecraft when pointed towards its reference position.

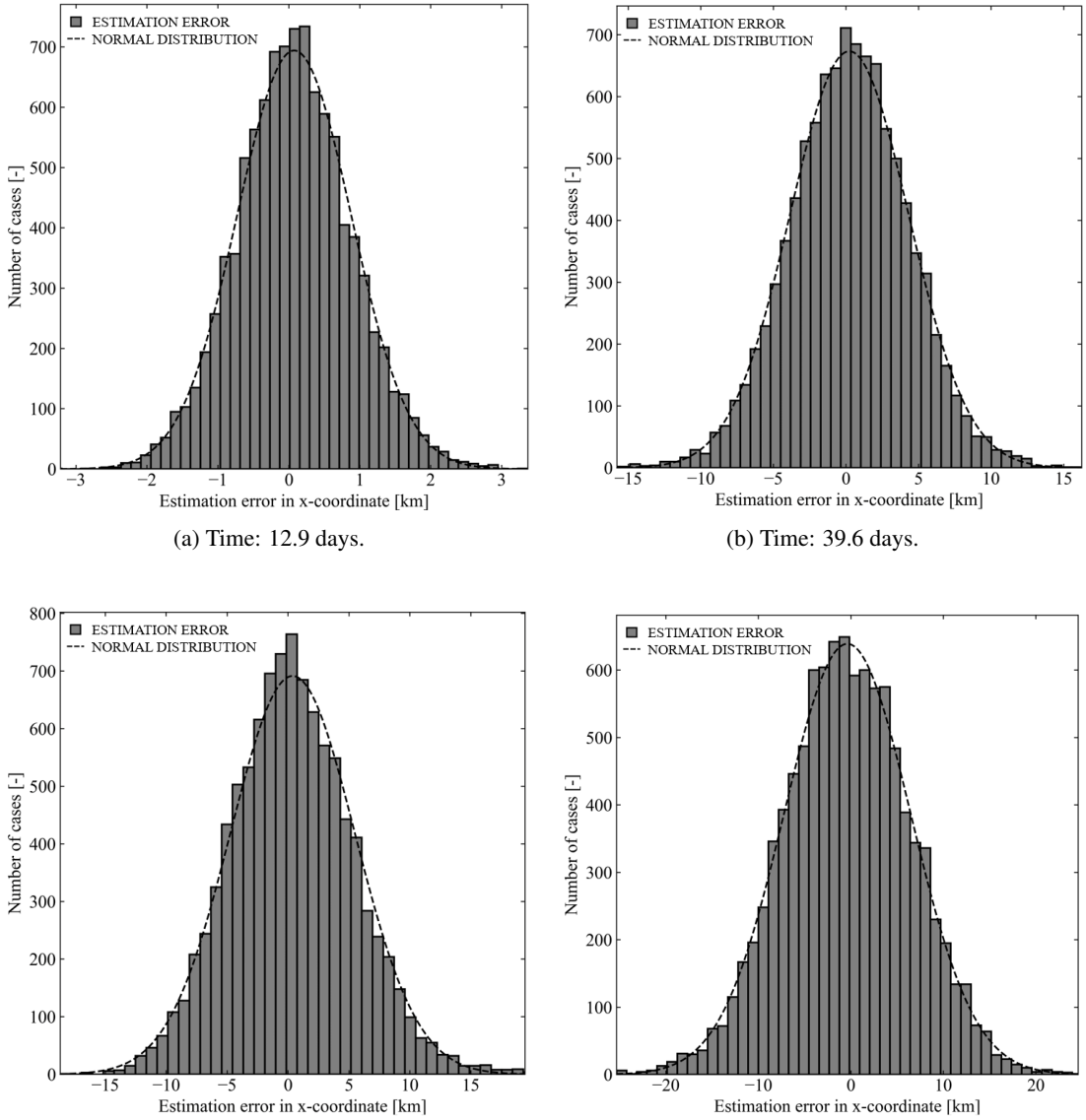

(a) Time: 12.9 days.

(b) Time: 39.6 days.

(c) Time: 66.3 days.

(d) Time: 106.4 days.

Fig. 6: Distribution of x-coordinate estimation error at various initial points for uncertainty propagation.

We consider 9 initial times $t_{0,i}$ ($i \in [1,9]$) for uncertainty propagation (Fig. 5), after which no new OD observations are collected. Leveraging the near-normal distribution of OD clouds of uncertainty, we introduce the simplifying assumption that the initial uncertainties can actually be perfectly described by correlated normally-distributed position and velocity components (i.e., nondiagonal covariance matrix). The correlation between variables is assumed to be the same as that computed at $t_{0,i}$ from the 10,000 OD Monte Carlo simulations (i.e., the orientation of the OD uncertainty ellipsoid is maintained), and the covariance matrix is scaled in such a way that the largest semi-axis of the uncertainty ellipsoid (i.e., square root of the largest eigenvalue) takes values 0.5 km, 2.5 km, 5.0 km and 10.0 km. These four rescaled covariance matrices are taken as representative examples of potential OD uncertainty magnitudes that may be encountered along the mission scenario (Fig. 5). We then forward-propagate these initial uncertainty clouds and analyze their behavior along time and depending on their initial size and initial time of propagation.

A total of 10,000 Monte Carlo cases are run for each initial size and initial time of propagation. Note, also, that

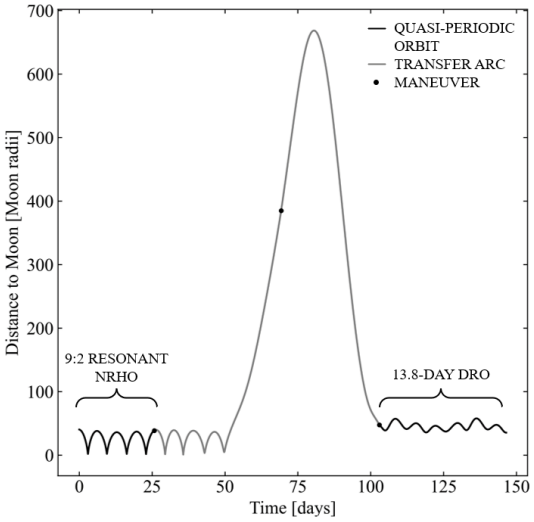

(a) Distance to Moon.

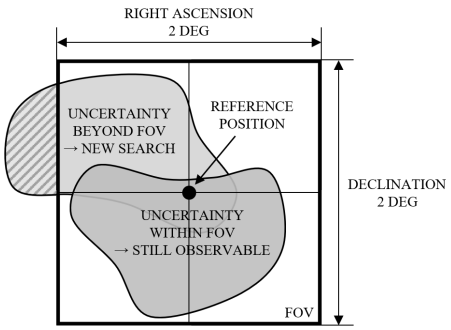

(b) Field of view.

Fig. 7: Distance to Moon along trajectory and ground-telescope field of view oriented towards reference spacecraft position.

our simulations assume that the spacecraft (each case in the Monte Carlo simulations) is still active and performs the remaining (if any) propulsive maneuvers nominally: i.e., no inaccuracies are introduced in the magnitude, direction or time of execution of the maneuvers. One could expect different evolutions of the clouds of uncertainty if maneuvers introduce execution errors, and, especially, if maneuvers are not executed (e.g., insertion maneuver into the transfer arc or into the arrival orbit). These cases, however, are not considered in our simulations and we solely analyze the effect and evolution of initial OD uncertainties.

Fig. 8 illustrates the geometrical evolution of uncertainty clouds along time, for the 9 different initial times of propagation $t_{0,i}$ (rows in Fig. 8) and four different initial uncertainty sizes (shades of grey in Fig. 8). Note that these clouds of uncertainty grow in size along time, but they are scaled in Fig. 8 for a qualitative illustration of the uncertainty evolution. Fig. 8 specifically illustrates the planar distribution (xy coordinates in the synodic reference frame) of uncertainty clouds at various times along the trajectory.

It is observed that, uncertainty clouds, initially obeying correlated normal distributions, evolve, first, into elongated, banana-shaped distributions (as typically displayed by uncertainties in the two-body problem). Then, as uncertainty clouds grow in size, the nonlinearity and chaoticity of the dynamical system come into play and greatly disturb the geometry of the uncertainty. Such unpredictable behaviors of uncertainty begin to appear approximately 80 days into the uncertainty propagation.

More insight on the evolution of uncertainty is provided in Fig. 9. Fig. 9a, for instance, illustrates the evolution of the 99th-percentile distance relative to the reference trajectory, with notable increases in size at close Moon encounters (Fig. 7a), and values that may reach up to 10^5 km depending on the time of propagation and initial propagation size. This highlights the importance of tracking and maintaining a catalog of cislunar objects, since their trajectories may evolve into large, unpredictable clouds of uncertainty if not observed frequently enough.

A Henze-Zirkler multivariate normality test is performed on the position coordinates and results are illustrated in Fig. 9b. Values above 0.05 correspond to position coordinates that may be appropriately described by correlated normal distributions. The normality test is passed for approximately 40 days, after which, clouds of uncertainty do not confidently adhere to normal distributions. Normality is a core assumption in an EKF, and, therefore, new observations should be collected with sufficient frequency to maintain normality in these clouds of uncertainty. Statistical quantities, kurtosis and skewness, to describe the shape of clouds of uncertainty are also illustrated in Figs. 9c and 9d, in this case, associated to the x position coordinate in the synodic reference frame. A kurtosis value of 3 and skewness of 0 correspond to normally-distributed variables. Kurtosis values above 3 correspond to more sharply peaked distributions, and lower values correspond to flatter curves. Positive skewness values correspond to a longer tail towards positive

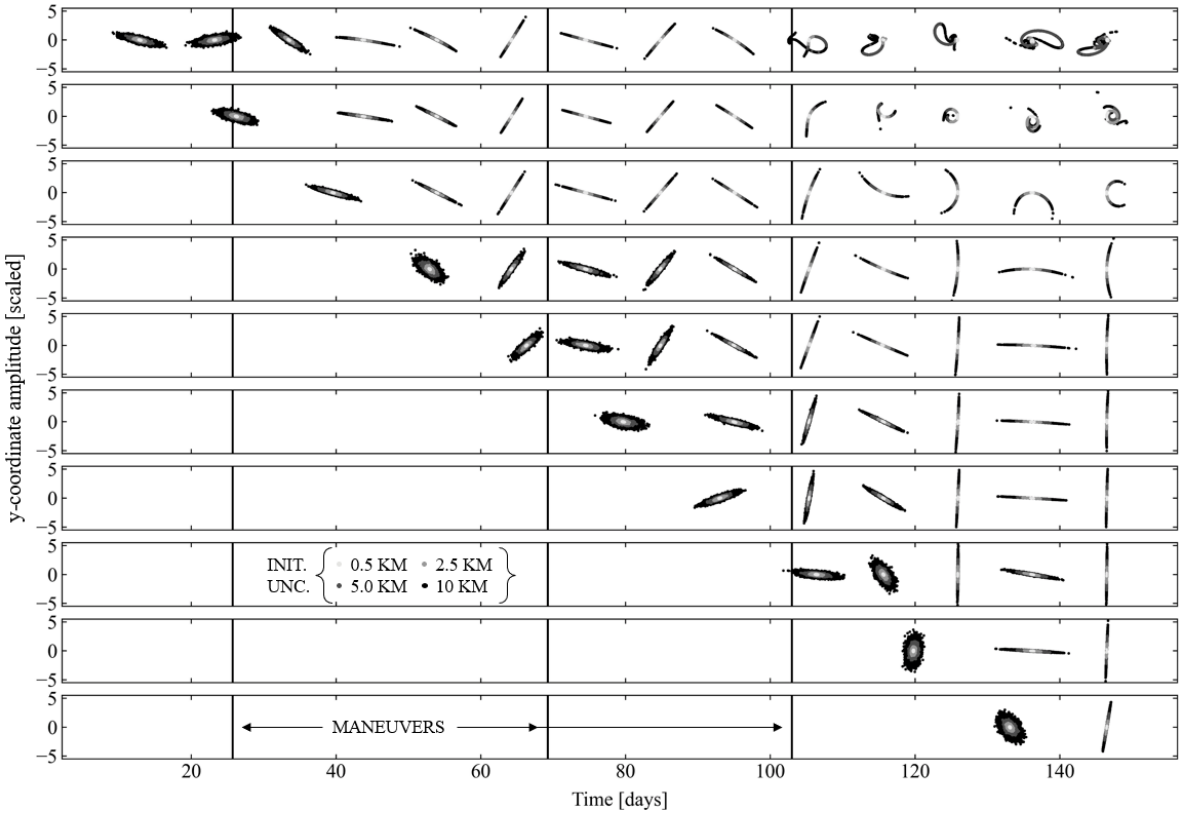

Fig. 8: Geometrical distribution of propagated clouds of uncertainty along time.

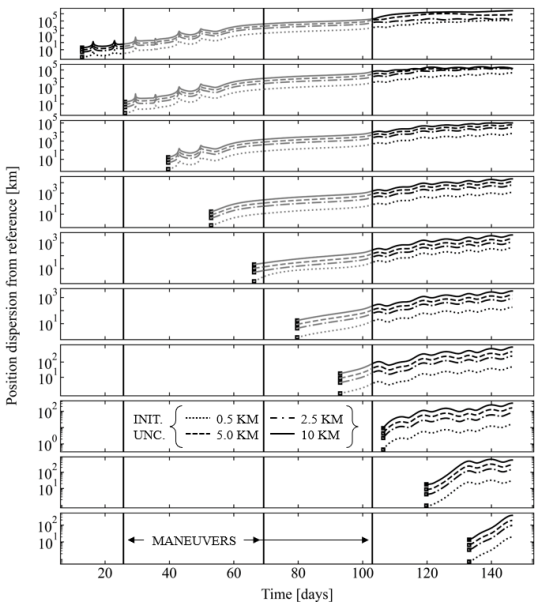

(a) 99th-percentile position uncertainty size.

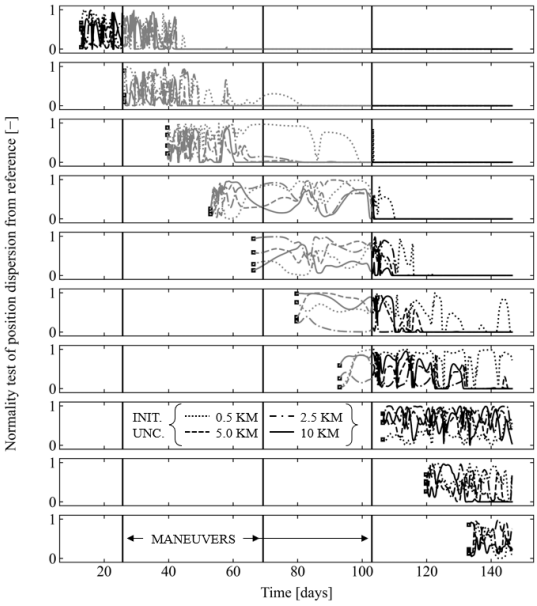

(b) Normality test of position coordinates.

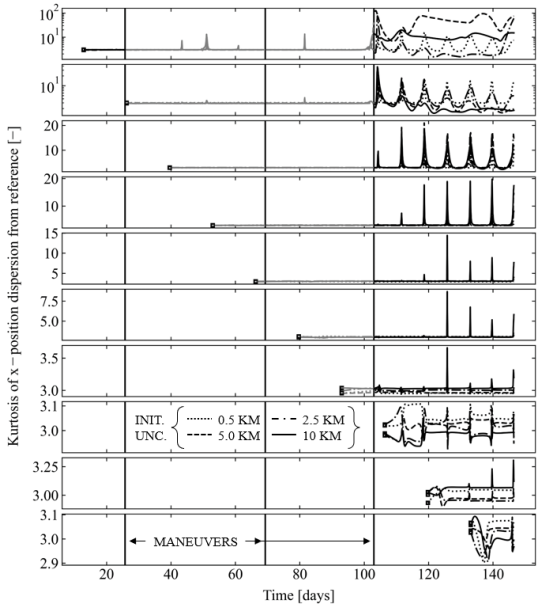

(c) Kurtosis of x-coordinate.

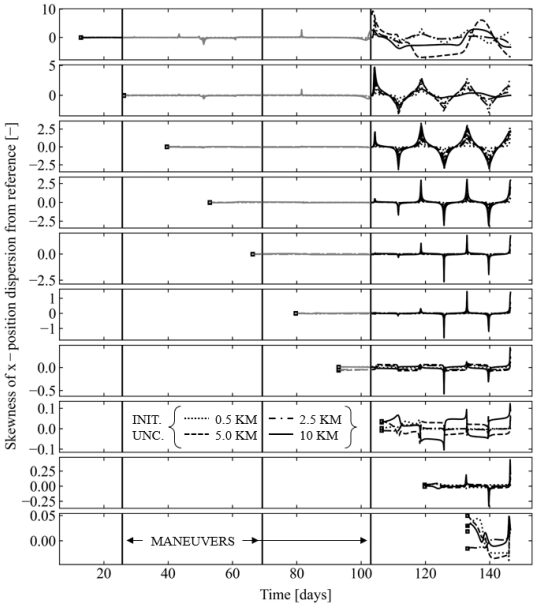

(d) Skewness of x-coordinate.

Fig. 9: Evolution of propagated OD uncertainty.

x-coordinates, and *vice versa*. In conjunction with Fig. 7a, it is clear that close Moon and Earth passages affect the geometry of these clouds of uncertainty, with large spikes both in kurtosis and skewness in these regions.

A similar trend can also be seen when measuring the observability of clouds of uncertainty. Fig. 10 illustrates the evolution of the 1st and 99th percentiles in right ascension and declination relative to the nominal observation orientation (Fig. 7b). It is observed again how close lunar passages result in larger right ascension and declination values, corresponding to clouds of uncertainty that cover a larger portion of the nominal field of view of the ground telescope; and the opposite is observed at apolune. Values above 1 deg in magnitude correspond to clouds of uncertainty that expand beyond the nominal field of view, effectively representing a larger probability that the unobserved spacecraft may be outside the nominal of view when trying to observe it again: i.e., it may be necessary for the ground telescope to search for the object again. Observability depends on the initial size of uncertainty and time of propagation, and it is maintained in this scenario for approximately 80 days.

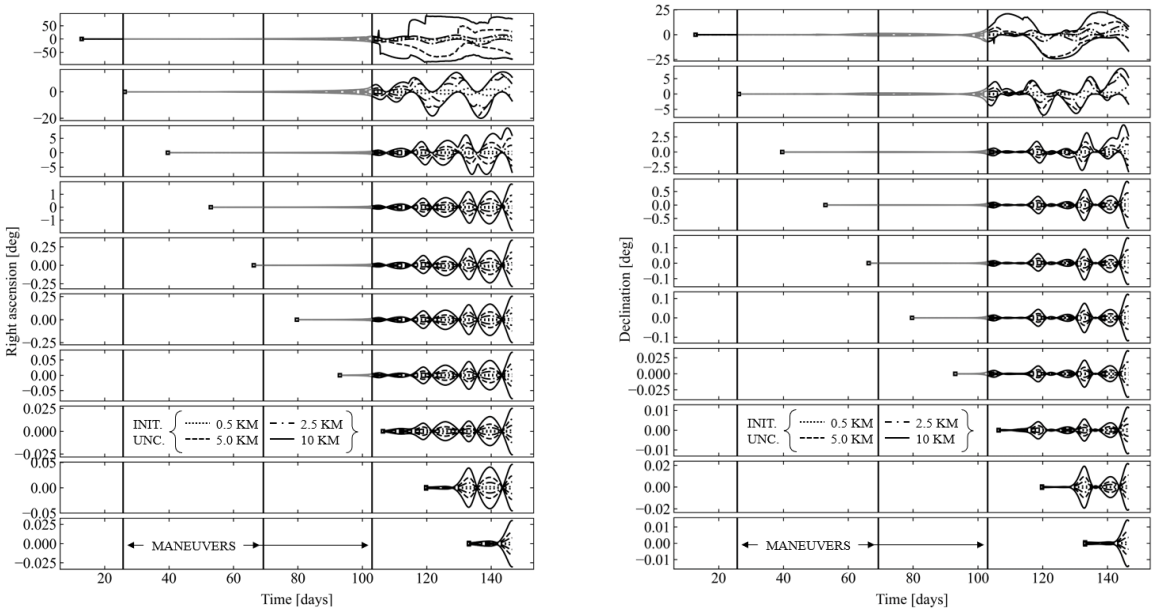

(a) Right ascension.

(b) Declination.

Fig. 10: Observability of clouds of uncertainty (1st and 99th percentiles).

5. CONCLUSIONS

In an effort to shed some light on the implications of the multi-body cislunar environment for space domain awareness, we explore a parametrization approach for scenarios of interest based on piecewise orbital-element representation, and propagate uncertainties involved in the orbit determination process to assess their effect on required revisit rates and surveillance volumes for cislunar catalog maintenance.

Orbital elements are shown to provide an intuitive and familiar representation, especially of (quasi-) periodic orbits, and the proposed piecewise approach with switches between geocentric and selenocentric orbital elements allows for a time-continuous representation of scenarios of interest. Positional orbit-determination uncertainties commonly range from 0.5 to 10 km and are primarily driven by the availability, frequency, and geometry of ground-based observations. Orbit determination uncertainties may evolve into large, highly perturbed clouds of uncertainty if objects are not observed with frequency. In particular, normality of uncertainties is maintained for approximately 40 days, and clouds of uncertainty remain within the nominal field of view of a ground telescope for approximately 80 days. Close Earth and Moon encounters are also shown to most significantly affect the shape and size of such clouds of uncertainty.

Results, although limited to the scenarios and assumptions here introduced, highlight the relevance of catalog maintenance of cislunar objects, and identify various areas for future research such as parametrization approaches for intuitive

representation of motion, maneuver detection and collision avoidance, computationally-efficient propagation of uncertainties, or dynamical systems approaches to characterize the evolution of uncertainties in the dynamically-complex cislunar environment.

REFERENCES

[1] D. Chongrui, M. K. Fain, and O. L. Starinova, "Analysis and design of halo orbits in cislunar space," *IOP Conference Series: Materials Science and Engineering* **984** (2020), 1–11.

[2] S. Trofimov, M. Shirobokov, A. Tselousova, and M. Ovchinnikov, "Transfers from near-rectilinear halo orbits to low-perilune orbits and the Moon's surface," *Acta Astronautica* **167** (2020), 260–270.

[3] M. Bolliger, M. R. Thompson, et al., "Ground-based navigation trades for operations in Gateway's near-rectilinear halo orbit," *Proceedings of the AAS/AIAA Space Flight Mechanics Conference*, Paper AAS 21-450 (2021), 1–16.

[4] R. E. Pritchett, E. Zimovan, K. Howell, "Impulsive and low-thrust transfer design between stable and nearly-stable periodic orbits in the restricted problem," *Proceedings of the 2018 Space Flight Mechanics Meeting*, Paper AIAA 2018-1690 (2018), 1–23.

[5] S. Yun, K. Tuggle, R. Zanetti, and C. D'Souza, "Sensor configuration trade study for navigation in near-rectilinear halo orbits," *The Journal of the Astronautical Sciences* **67** (2020), 1755–1774.

[6] N. H. Crisp, K. Smith, and P. Hollingsworth, "Launch and deployment of distributed small satellite systems," *Acta Astronautica* **114** (2015), 65–78.

[7] W. J. Faccenda, "GEODSS: Past and Future Improvements," *The MITRE Corporation* (2020), 1–7.